13. Murdoch, J. N. *et al.* Disruption of scribble (Scrb1) causes severe neural tube defects in the circletail mouse. *Hum. Mol. Genet.* **12,** 87–98 (2003).
14. Hung, N. Y. & Sheng, M. PDZ domains: structural molecules for protein complex assembly. *J. Biol. Chem.* **277,** 5699–5702 (2002).
15. Mlodzik, M. Planar cell polarization: do the same mechanisms regulate *Drosophila* tissue polarity and vertebrate gastrulation? *Trends Genet.* **18,** 564–571 (2002).
16. Park, M. & Moon, R. T. The planar cell-polarity gene stbm regulates cell behaviour and cell fate in vertebrate embryos. *Nature Cell. Biol.* **4,** 20–25 (2002).
17. Chen, P., Johnson, J. E., Zoghbi, H. Y. & Segil, N. The role of Math1 in inner ear development: uncoupling the establishment of the sensory primordium from hair cell fate determination. *Development* **129,** 2495–2505 (2002).
18. Hamblet, N. S. *et al.* Dishevelled 2 is essential for cardiac outflow tract development, somite segmentation and neural tube closure. *Development* **129,** 5827–5838 (2002).
19. Bilder, D. & Perrimon, N. Localization of apical epithelial determinants by the baso-lateral PDZ protein scribble. *Nature* **403,** 676–680 (2000).
20. Darken, R. S. *et al.* The planar polarity gene *strabismus* regulates convergent extension movements in *Xenopus*. *EMBO J.* **21,** 976–985 (2002).
21. Goto, T. & Keller, R. The planar cell polarity gene strabismus regulates convergence and extension and neural fold closure in *Xenopus*. *Dev. Biol.* **247,** 165–181 (2002).
22. Copp, A. J., Checiu, I. & Henson, J. N. Developmental basis of severe neural tube defects in the *loop-tail* (*Lp*) mutant mouse: use of microsatellite DNA markers to identify embryonic genotype. *Dev. Biol.* **165,** 20–29 (1994).
23. Mueller, K. L., Jacques, B. E. & Kelley, M. W. Fibroblast growth factor signaling regulates pillar cell development in the organ of Corti. *J. Neurosci.* **22,** 9368–9377 (2002).
24. Lanford, P. J. *et al.* Notch signalling pathway mediates hair cell development in mammalian cochlea. *Nature Genet.* **21,** 289–292 (1999).
25. Wu, D. K. & Oh, S. H. Sensory organ generation in the chick inner ear. *J. Neurosci.* **16,** 6454–6462 (1996).

Acknowledgements We thank J. Jones for assistance with *in situ* hybridization and C. Woods for technical support. We also thank R. Wenthold, N. Sans, I. Belyantseva, D. Forrest, A. Dabdoub, J. Jones and R. Hertzano for reading an earlier version of this manuscript. This research was supported by funds from the Intramural Programs at NIDCD and NCI.

Competing interests statement The authors declare that they have no competing financial interests.

Correspondence and requests for materials should be addressed to M.M. (montcouq@nidcd.nih.gov).

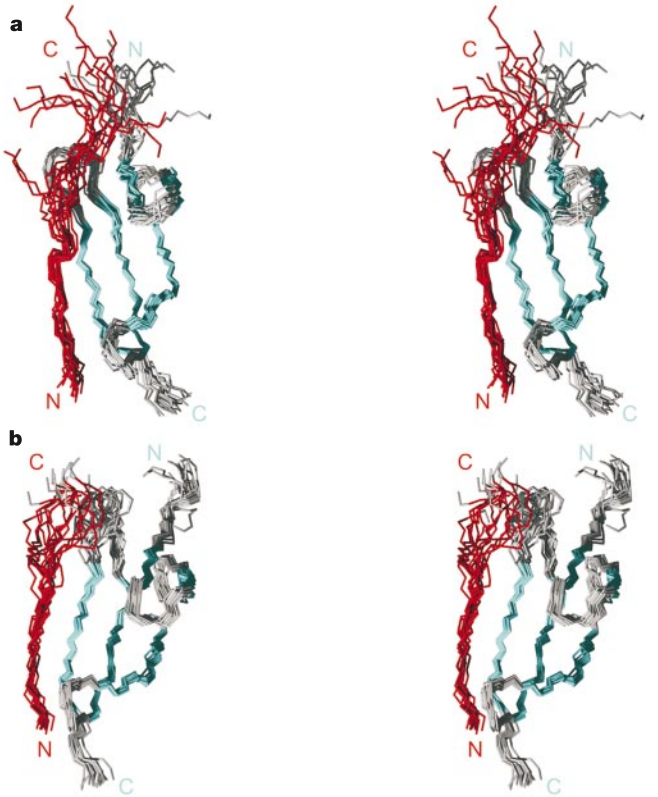

Figure 1 Family of NMR-derived structures of the ^{1}F1^{2}F1 module pair from human Fn complexed with B3 from *S. dysgalactiae* (Table 1). Stereo view of structures overlaid on the backbone Cα atoms of the F1 β-strands of ^{1}F1–B3(1052–1066) (**a**) and ^{2}F1–B3(1043–1051) (**b**). F1 β-strands and B3 residues are shown in cyan and red, respectively. The N and C termini of ^{1}F1, ^{2}F1 (cyan) and B3 regions (red) are indicated.

Pathogenic bacteria attach to human fibronectin through a tandem β-zipper

Ulrich Schwarz-Linek*, Jörn M. Werner*, Andrew R. Pickford*, Sivashankarappa Gurusiddappa†, Jung Hwa Kim†, Ewa S. Pilka*, John A. G. Briggs*‡, T. Sebastian Gough*, Magnus Höök†, Iain D. Campbell*§ & Jennifer R. Potts*

* *Department of Biochemistry, University of Oxford, South Parks Road, Oxford OX1 3QU, UK*
† *Center for Extracellular Matrix Biology, Institute of Biosciences and Technology, Texas A&M University System Health Science Center, Houston, Texas 77030-3303, USA*
§ *Oxford Centre for Molecular Sciences, Central Chemistry Laboratory, University of Oxford, South Parks Road, Oxford OX1 3QH, UK*

***Staphylococcus aureus* and *Streptococcus pyogenes*, two important human pathogens, target host fibronectin (Fn) in their adhesion to and invasion of host cells[1,2]. Fibronectin-binding proteins (FnBPs), anchored in the bacterial cell wall, have multiple Fn-binding repeats[3] in an unfolded[4,5] region of the protein. The bacterium-binding site in the amino-terminal domain ($^{1-5}$F1) of Fn contains five sequential Fn type 1 (F1) modules. Here we show the structure of a streptococcal (*S. dysgalactiae*) FnBP peptide (B3)[6,7] in complex with the module pair ^{1}F1^{2}F1. This identifies ^{1}F1- and ^{2}F1-binding motifs in B3 that form additional antiparallel β-strands on sequential F1 modules—the first example of a tandem β-zipper. Sequence analyses of larger regions of FnBPs from *S. pyogenes* and *S. aureus* reveal a repeating pattern of F1-binding motifs that match the pattern of F1 modules in $^{1-5}$F1 of Fn. In the process of Fn-mediated invasion of host cells, therefore, the bacterial proteins seem to exploit the modular structure of Fn by forming extended tandem β-zippers. This work is a vital step forward in explaining the full mechanism of the integrin-dependent[2,8] FnBP-mediated invasion of host cells.**

Fn and Fn–integrin interactions are required for normal physiological processes. Bacterial FnBP-mediated adhesion to and integrin-dependent invasion of host cells therefore seem to be examples of the exploitation of host cell processes by pathogens[9]. Internalization might aid evasion of the immune system and administered antibiotics by allowing bacteria to 'hide' inside host cells. In addition, as bacteria must cross the endothelial lining to enter or leave the vasculature, internalization might assist the haematogenous dissemination of infection to other tissues, which is a characteristic of invasive infection by *S. aureus*[10]. In support of this, FnBPs are central to the interaction of *S. aureus* with endothelial cells *in vitro*[1,8]. FnBPs also mediate the attachment of bacteria to implanted material, which becomes coated with host proteins[11], indicating a possible role in infections associated with catheters and prosthetic devices. The absence of three-dimensional structural information until now has precluded an explanation of the mechanism by which the largely unstructured Fn-binding repeats of FnBPs[4,5] recognize $^{1-5}$F1.

The structure of the ^{1}F1^{2}F1–B3 complex (Fig. 1) was determined by NMR spectroscopy. In the family of structures (Fig. 1), the

‡ Present address: Division of Structural Biology, The Wellcome Trust Centre for Human Genetics, Roosevelt Drive, Headington, Oxford OX3 7BN, UK.

individual F1 modules are well defined (Table 1) and retain the structure of the free F1 module, characterized by a β-sandwich of two antiparallel β-sheets; a double-stranded sheet (strands A and B) followed by a triple-stranded sheet (strands C, D and E; Fig. 2)[12]. On binding to the module pair, the bacterial peptide contributes a fourth antiparallel strand to the triple-stranded β-sheet of sequential F1 modules in a tandem β-zipper interaction. In NMR spectra of the complex, Hα–Hα intermolecular distances typical of β-sheet formation were observed for residues shown in italics in the sequences below.

The complex reveals two different F1 recognition sequences within B3 and their molecular character is mirrored by the properties of the two F1 interaction surfaces. The carboxy-terminal L*SIH*FDNE**WP** part of the B3 peptide binds along a wide groove on the surface of the ^{1}F1 module bounded by the C–D and D–E loops (Fig. 2a). The alternating hydrophobic side chains of the peptide residues underlined above interact with a hydrophobic patch formed largely by Tyr 38 in the C–D loop and Leu 43 in strand D. Additional interactions are observed between Tyr 22 in the A strand of ^{1}F1 and the B3 residues in bold above. The presence of the [I/F]HFDNX(X)P motif in streptococcal FnBPs has been noted previously[13]. However, as this sequence only occurs once within each protein it has not usually been considered part of the Fn-binding repeat regions. The ^{1}F1^{2}F1–B3 structure reveals the role of this motif in binding ^{1}F1.

In comparison with ^{1}F1, the surface of the peptide-binding region of ^{2}F1 is more basic (Fig. 2a). This is due to the presence of Lys 85 in the C–D loop of ^{2}F1 (in a homologous position to Tyr 38 in ^{1}F1), Arg 101 in the D–E loop and Lys 69 in the A strand[12]. The region of B3 binding to ^{2}F1 contains the sequence *ST*T*EV***ED**[**S/T**]. The residues in bold are conserved in FnBPs from Gram-positive bacteria[6] and in the structure are in close proximity to the positively charged region of the ^{2}F1 surface (Fig. 2a); thus electrostatic interactions are likely to be important in the binding. The residues underlined above in the ^{1}F1- and ^{2}F1-binding regions of B3 are highlighted in Fig. 2a.

The directionality of the peptide binding is encoded in the antiparallel β-sheet extension of the individual F1 modules and can be best appreciated in the structure of the module pair. Figure 2 shows an elongated conformation for the ^{1}F1^{2}F1–B3 complex as is observed in most (14 of 15) structures in the family shown in Fig. 1. The inter-module orientation is significantly better defined in the complex with B3 than in the free form[12], indicating that B3 might tether the two F1 modules. However, a degree of variability remains in the inter-module orientation even after the inclusion in the structure calculations of long-range restraints based on residual dipolar couplings and ^{15}N-relaxation rates.

The structure reveals (1) β-strand formation (a β-zipper) as a mechanism of F1 module recognition; (2) an antiparallel orientation for Fn and FnBP; (3) the approximate length (about eight residues) of an F1-binding motif; (4) likely sources of F1-binding specificity in the F1 and peptide sequences; and (5) that B3 forms a tandem β-zipper on adjacent F1 modules. The combination of these results with sequence analyses of homologous FnBPs and previous results[7,14] leads to a novel model for binding of *S. pyogenes* and *S. aureus* to $^{1-5}$F1 (Fig. 3).

The C-terminal regions of the FnBPs SfbI (from *S. pyogenes*[15]) and FnBPA (from *S. aureus*[16]) can be arranged into 5 and 11 segments (SfbI-1 to SfbI-5 and FnBPA-1 to FnBPA-11), respectively, such that each (except FnBPA-7) contains a similar series of putative F1-binding motifs. The definition of the F1-binding motifs is assisted by sequence conservation between the segments and between SfbI, FnBPA and other FnBPs (data not shown), but it is clear that the sequences of some motifs are more conserved than others. Each segment in SfbI contains motifs in the correct order to bind sequential F1 modules in $^{2-5}$F1 or $^{1-5}$F1. The motifs are predicted to bind F1 modules primarily by forming a β-strand along the E strand of the triple-stranded β-sheet in a similar manner to the B3 interaction with ^{1}F1^{2}F1 shown in Fig. 1. However, in the

Table 1 **Experimental restraints and structural statistics**

Number of experimental restraints			
	^{1}F1^{2}F1	B3	Intermolecular
NOEs	1279	157	127
Hydrogen bonds	7		
TALOS (φ/ψ)	76		
^{15}N relaxation restraints	29		
^{15}N–^{1}H RDC restraints	40		
R.m.s.d. from experimental restraints (means ± s.d.)			
Distance (Å)	0.020 ± 0.002		
Angles (degrees)	0.39 ± 0.08		
Hydrogen bond (Å)	0.010 ± 0.006		
R.m.s.d. from idealized covalent geometry (means ± s.d.)			
Bonds (Å)	0.0020 ± 0.0001		
Angles (degrees)	0.319 ± 0.016		
Impropers (degrees)	0.38 ± 0.02		
R.m.s.d. of cartesian coordinates (means ± s.d.)			
	^{1}F1–B3	^{2}F1–B3	^{1}F1^{2}F1*
Backbone (Å)	0.50 ± 0.08	0.49 ± 0.12	1.13 ± 0.31
All heavy atoms (Å)	0.97 ± 0.10	0.96 ± 0.20	1.42 ± 0.29

Fifteen structures were chosen on the basis of low overall energy. None of the structures showed experimental distance or angle violations of more than 0.3 Å or more than 3°, respectively. Root-mean-square deviation (r.m.s.d.) calculations were performed over β-strand residues of the F1 modules[12] and for B3 residues 23–28 (binding to ^{1}F1) and 13–18 (binding to ^{2}F1). The 14 low-energy structures showed an elongated conformation in the complex.
*Structure 15 had a different intermodular orientation, resulting in lower consistency with RDC restraints. This structure was not included in the overlay of both modules.

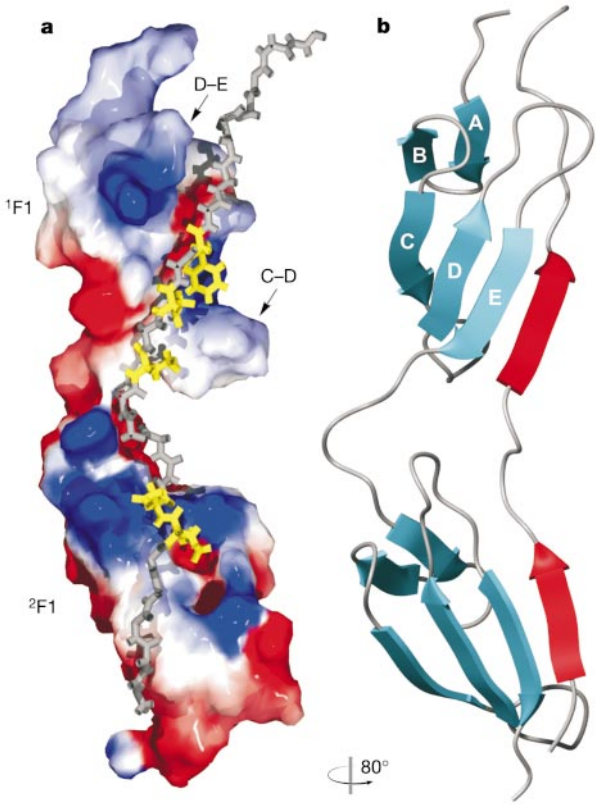

Figure 2 Molecular surface (prepared using GRASP) and ribbon diagram (prepared with MOLMOL) of ^{1}F1^{2}F1–B3. **a**, Surface potential of ^{1}F1^{2}F1 shown on the lowest-energy structure from Fig. 1 with bound B3 (grey). Negatively and positively charged regions of the ^{1}F1^{2}F1 surface are shown in red and blue, respectively. Side chains of hydrophobic and acidic B3 residues (yellow) are mentioned in the text. **b**, Ribbon diagram of the lowest-energy structure showing β-strands of the F1 modules (cyan) and the fourth strand formed by B3 (red). The definition of the sheet extension is based on characteristic cross-peaks in NOESY spectra and changes in ^{1}H NMR chemical shifts[29]. The difference in orientation between the two views is indicated. F1 β-strand labels are shown on ^{1}F1.

^{1}F1- and ^{2}F1-binding motifs the β-strand-forming residues are not the most conserved, indicating that additional F1-binding specificity might arise from interactions of the side chains of conserved residues with the F1 modules. This is supported by the observation of interactions between B3 and ^{1}F1 A-strand residues (Fig. 1) in the NMR spectra of the ^{1}F1^{2}F1–B3 complex[17] (see above). In FnBPA, the pattern of motifs and previous data[6,14] suggest a similar mechanism of binding to the N-terminal domain of Fn. However, there is no obvious ^{1}F1-binding motif in FnBPA, and the lack of sequence conservation indicates that some segments might not bind ^{5}F1.

The extended tandem β-zipper model described above was tested experimentally (Fig. 3). Peptides from SfbI containing putative ^{1}F1^{2}F1-, ^{2}F1^{3}F1- and ^{4}F1^{5}F1-binding sites were shown to bind to their predicted module pair targets. When the predicted binding sites *in vivo* are intact (SfbI-5 and $^{1-5}$F1), the lower-affinity interactions involving F1 module pairs combine to form a high-affinity multipoint interaction (Fig. 3). It should be noted that the interaction between SfbI-4 or SfbI-5 and $^{1-5}$F1 is weaker than predicted by the product of the K_d values (measured at low ionic strength) for the interactions of the subdomains. This is likely to be due to the dependence of the interactions on ionic strength (data not shown). At lower ionic strength (see Methods) the affinity of the interaction between SfbI-4 or SfbI-5 and $^{1-5}$F1 would have been too high to measure directly by isothermal titration calorimetry (ITC). Synthetic peptides from FnBPA were also shown to bind to ^{2}F1^{3}F1 and ^{4}F1^{5}F1 as predicted. The specificity of the ^{4}F1^{5}F1-binding peptide has been demonstrated previously[7,18]. The ^{2}F1^{3}F1-binding motif from FnBPA-1 is outside the traditionally defined Fn-binding repeats in FnBPA[16] (Fig. 3) and is a strong test of the model. The existence of binding sites for Fn near the C terminus of the A domain (Fig. 3) has been demonstrated recently[19].

In addition to the ^{1}F1^{2}F1–B3 structure, further evidence of the formation of a β-zipper along the E strand of the F1 modules comes from changes in ^{2}F1^{3}F1 (data not shown) and ^{4}F1^{5}F1 (ref. 14) backbone NMR chemical shifts when the FnBP peptide binds. In the model (Fig. 3), SfbI and FnBPA contain multiple binding sites for $^{2-5}$F1. SfbI also contains a single $^{1-5}$F1-binding site near the C terminus of the protein. Thus, the extended tandem β-zipper model is consistent with earlier studies indicating that D1–D3 from FnBPA (Fig. 3) binds two molecules of $^{1-5}$F1 with high (nanomolar) affinity[18] and that FnBPA contains multiple substituting binding sites for Fn[19]. The common themes in streptococcal and staphylococcal Fn binding identified here (despite the lack of an obvious ^{1}F1-binding motif in FnBPA) are consistent with the ability of peptides from streptococcal FnBPs to inhibit the binding of *S. aureus* to Fn[6]. The model also provides a plausible mechanism for the propagation of a conformational change along SfbI that could explain the apparent activation of UR domain (Fig. 3) binding to the Fn gelatin-binding domain[20].

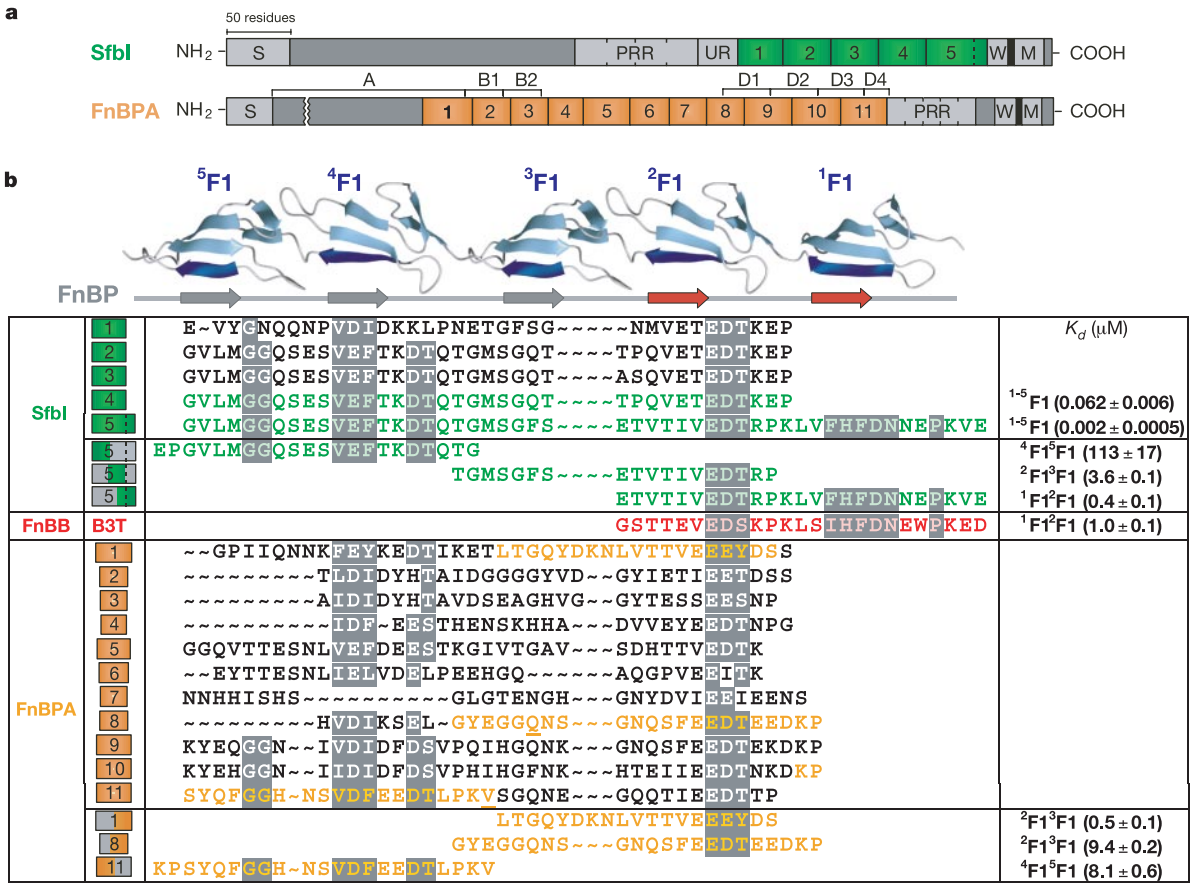

Figure 3 The extended tandem β-zipper model. **a**, Schematic representations of SfbI[15,30] and FnBPA[16] showing putative $^{1-5}$F1-binding segments (green and orange boxes). For FnBPA, the locations of the traditionally defined regions (A, B and D) are also shown. The first and last residues of D1–D3 are underlined in **b**. Other terms are explained in Talay *et al.*[30] and Swiss-Prot entry P14738. **b**, The extended tandem β-zipper model is at the top. A $^{1-5}$F1-binding segment is shown as a grey line with short β-strands along the E strand (shown in navy blue) of five sequential modules with the consensus F1 fold (ref. 12; cyan). FnBP β-strands for which three-dimensional structural data are available (Fig. 1) are shown in red. The position of the F1 modules approximates the location of F1-specific motifs in the segments aligned below. Peptides used in testing the model and the K_d values for the interactions are shown. The location of these peptides in the segments is also indicated. B3T (red) contains all the ^{1}F1^{2}F1-binding residues of B3 and binds with similar affinity[17].

The formation of intermolecular or subunit interfaces through the extension of a β-sheet (a β-zipper interaction) has been observed on several occasions, for example in an interaction involving an IgG-binding protein[21]. Here we have identified the first tandem β-zipper interaction, where β-strands are formed on adjacent domains, and we also provide evidence that this is part of an extended tandem β-zipper that forms on the binding of larger regions of the bacterial and host proteins. As well as showing how pathogenic bacteria can adhere to F1 modules in $^{1-5}$F1 of Fn, the consequences of the mechanism, namely the high affinity and specificity of the binding, the significant conformational change undergone by the unfolded region of the FnBP and the presence of multiple Fn-binding sites, are all likely to have a role in bacterial invasion. This work is therefore a significant step towards the goal of understanding this process. □

Methods

Recombinant expression and peptide synthesis

Production of the *P. pastoris* clones expressing ^{1}F1^{2}F1 and ^{4}F1^{5}F1 (residues 17–109 and 152–244, respectively, of mature human Fn) have been described previously[12]. The clone expressing ^{2}F1^{3}F1 (residues 62–151 of mature human Fn) was produced in an analogous fashion. Unlabelled ^{1}F1^{2}F1, ^{2}F1^{3}F1 and ^{4}F1^{5}F1, uniformly ^{15}N-labelled ^{1}F1^{2}F1 ([U-^{15}N]^{1}F1^{2}F1) and ^{4}F1^{5}F1 ([U-^{15}N]^{4}F1^{5}F1), and uniformly ^{13}C/^{15}N-labelled ^{1}F1^{2}F1 ([U-^{13}C^{15}N]^{1}F1^{2}F1) were expressed in fermenters by using established methods[12,22]. For the expression of uniformly ^{2}H/^{15}N-labelled ^{1}F1^{2}F1 ([U-^{2}H^{15}N]^{1}F1^{2}F1), the *P. pastoris* cells were conditioned for growth in perdeuterated medium by sequentially subculturing mid-exponential phase cells from unlabelled buffered minimal glycerol medium[22] into medium containing 50%, 80% or 100% $^{2}H_2O$. These cells were fermented in perdeuterated basal salts medium containing *Pichia* trace minerals, 1% (w/v) $(^{15}N^{2}H_4)_2SO_4$ and 0.5% (w/v) [^{2}H]glycerol. On depletion of the carbon source, ^{1}F1^{2}F1 expression was induced with 1% (v/v) [^{2}H]methanol. ^{1}F1^{2}F1, ^{2}F1^{3}F1 and ^{4}F1^{5}F1 were purified and characterized much as described previously[12]. Segments encoding SfbI-4 and SfbI-5 were amplified by PCR from *S. pyogenes* M75 DNA (4673) using the oligonucleotides 5′-GCGGGATCCCCGGAGTATTGATGGGAGGTCAAAGT-3′, and for SfbI-4: 5′-GCGCTCGAGTCATGGCTCTTTCGTGTCTTCTGTCTC-3′, or for SfbI-5: 5′-GCGCTCGAGTCATTCCACTTTGGGCTCATTATTGTC-3′. The amplified PCR product was digested with *Bam*HI and *Xho*I and ligated into appropriately digested pGEX-5X-1 (Amersham Pharmacia Biotech). Transformed *Escherichia coli* JM101 cells with insert were picked and grown on plates made with Luria–Bertani medium containing ampicillin (100 μg ml^{-1}; LB-Amp). Recombinant glutathione *S*-transferase (GST) fusion protein was expressed and purified in accordance with the manufacturer's instructions with slight modification. Overnight culture of transformant was diluted 1:25 in LB-Amp and incubated at 37 °C with shaking until D_{600} reached 0.7. Expression was induced for 4 h by adding isopropyl β-D-thiogalactopyranoside (Invitrogen) to a final concentration of 0.2 mM. The GST fusion protein was purified from lysates on a glutathione–agarose column (Sigma). GST was cleaved off with Factor Xa (New England Biolabs), and the peptide (residues 505–541 or 542–591 of SfbI for SfbI-4 and SfbI-5, respectively, with three non-native N-terminal residues, Gly-Ile-Pro) was purified by reverse-phase high-performance liquid chromatography (HPLC). B3 (EESLPTEQGQSGSTTEVEDSKPKL SIHFDNEWPKED; residues 1031–1066) from *S. dysgalactiae* FnBB and other peptides were synthesized in house or obtained from Alta Bioscience. Residue numbers for the ^{1}F1^{2}F1-, ^{2}F1^{3}F1- and ^{4}F1^{5}F1-binding peptides from SfbI-5 are 567–591, 560–577 and 540–561, respectively. Residue numbers for ^{2}F1^{3}F1-binding peptides from FnBPA-1 and FnBPA-8 are 531–549 and 741–762, respectively. Residue numbers for the ^{4}F1^{5}F1-binding peptide from FnBPA-11 are 837–858. Peptides were purified by reverse-phase HPLC, and the mass was confirmed by electrospray or matrix-assisted laser desorption ionization mass spectrometry.

Structural restraints

Spectrometers were as described previously[12]. Standard two- and three-dimensional experiments, acquired at pH 5.0 and 25 °C or 10 °C, were used for the assignment and collection of restraints for structure calculations. Spectra of [U-^{15}N^{2}H]^{1}F1^{2}F1 with different B3 concentrations greatly assisted the assignment of bound B3. The following spectra of [U-^{13}C^{15}N]^{1}F1^{2}F1:B3T 1:2 were acquired to obtain C′ and Cα chemical shifts: HNCO, CCCONH, {^{13}C–^{1}H} constant-time heteronuclear single-quantum coherence (HSQC) and ^{13}C–^{1}H nuclear Overhauser enhancement spectroscopy (NOESY)-HSQC.

Intramolecular distance restraints for the module pair and peptide were collected from NOESY spectra of samples where ^{1}F1^{2}F1 or B3 was fully bound, respectively. Samples in which more than 80% ^{1}F1^{2}F1 and more than 98% B3 were bound were used for intermolecular restraints. NOE-based and hydrogen-bond distance restraints were collected and incorporated much as described previously[12]. Restraints derived from TALOS (Torsion angle likelihood obtained from shift and sequence similarity)[23] for ϕ and ψ angles were also used. Structure calculations were performed with a version of XPLOR 3.8 (ref. 24) provided by M. Clore. Residual dipolar couplings (RDCs) between backbone ^{1}H and ^{15}N atoms were measured for the [U-^{13}C^{15}N]^{1}F1^{2}F1–B3 complex within the aqueous phase of a polyacrylamide gel (4%) under radial compression[25]. The H–N couplings were measured as described previously[26]. Restraints based on ^{15}N relaxation data for the ^{1}F1^{2}F1–B3 complex were measured as described previously[27]. RDC and ^{15}N relaxation-based restraints[28] were introduced during the refinement stage. One hundred structures were calculated and the 15 lowest-energy structures were selected for analysis. Figures were prepared with MOLMOL (authors R. Koradi, M. Billeter and K. Wüthrich), POV-Ray and MegaPov (authors The POV-Ray team), GRASP (authors A. Nicholls, R. Bharadwaj and B. Honig; with full.crg charge file), Swiss-PdbViewer (authors N. Guex and M. C. Peitsch) and Raster3d (authors E. A. Merritt and M. E. P. Murphy).

Dissociation constants

K_d values for SfbI peptide binding to ^{1}F1^{2}F1 (pH 5.0) and ^{2}F1^{3}F1 (pH 7.4) and FnBPA peptide binding to ^{2}F1^{3}F1 (pH 7.4) and ^{4}F1^{5}F1 (pH 5.0) were measured at 25 °C by ITC in low-ionic-strength buffer as described previously[17]. The K_d for SfbI-4 or SfbI-5 binding to $^{1-5}$F1 was measured at physiological ionic strength at 25 °C or 37 °C, respectively, in an ITC experiment with the 30-kDa N-terminal fragment of Fn (7 μM or 2 μM, respectively; Sigma) and SfbI-4 (91 μM) or SfbI-5 (29 μM). The K_d for SfbI peptide binding to [U-^{15}N]^{4}F1^{5}F1 was measured by fitting changes in backbone ^{1}H and ^{15}N NMR chemical shifts to the following equation:

$$\Delta = \Delta_0 \frac{K_d + [L] + [P] - \sqrt{(K_d + [L] + [P])^2 - 4[L][P]}}{2[P]}$$

where Δ is the observed chemical shift change, Δ_0 is the total change in chemical shift at saturation, and [L] and [P] are the peptide and ^{4}F1^{5}F1 concentrations, respectively.

Received 20 December 2002; accepted 21 March 2003; doi:10.1038/nature01589.

1. Peacock, S. J., Foster, T. J., Cameron, B. J. & Berendt, A. R. Bacterial fibronectin-binding proteins and endothelial cell surface fibronectin mediate adherence of *Staphylococcus aureus* to resting human endothelial cells. *Microbiology* **145,** 3477–3486 (1999).
2. Ozeri, V., Rosenshine, I., Mosher, D. F., Fässler, R. & Hanski, E. Roles of integrins and fibronectin in the entry of *Streptococcus pyogenes* into cells *via* protein F1. *Mol. Microbiol.* **30,** 625–637 (1998).
3. Patti, J. M., Allen, B. L., McGavin, M. J. & Höök, M. MSCRAMM-mediated adherence of microorganisms to host tissues. *Annu. Rev. Microbiol.* **48,** 585–617 (1994).
4. House-Pompeo, K., Xu, Y., Joh, D., Speziale, P. & Höök, M. Conformational changes in the fibronectin binding MSCRAMMs are induced by ligand binding. *J. Biol. Chem.* **271,** 1379–1384 (1996).
5. Penkett, C. J. *et al.* Structural and dynamical characterization of a biologically active unfolded fibronectin-binding protein from *Staphylococcus aureus*. *Biochemistry* **37,** 17054–17067 (1998).
6. McGavin, M. J. *et al.* Fibronectin receptors from *Streptococcus dysgalactiae* and *Staphylococcus aureus*—involvement of conserved residues in ligand binding. *J. Biol. Chem.* **268,** 23946–23953 (1993).
7. Joh, D., Speziale, P., Gurusiddappa, S., Manor, J. & Höök, M. Multiple specificities of the staphylococcal and streptococcal fibronectin-binding microbial surface components recognizing adhesive matrix molecules. *Eur. J. Biochem.* **258,** 897–905 (1998).
8. Sinha, B. *et al.* Fibronectin-binding protein acts as *Staphylococcus aureus* invasin via fibronectin bridging to integrin $\alpha_5\beta_1$. *Cell. Microbiol.* **1,** 101–117 (1999).
9. Knodler, L. A., Celli, J. & Finlay, B. B. Pathogenic trickery: Deception of host cell processes. *Nature Rev. Mol. Cell Biol.* **2,** 578–588 (2001).
10. Ing, M. B., Baddour, L. M. & Bayers, S. A. in *The Staphylococci in Human Disease* (eds Crossley, K. B. & Archer, G. L.) 331–354 (Churchill Livingstone, New York, 1997).
11. Greene, C. *et al.* Adhesion properties of mutants of *Staphylococcus aureus* defective in fibronectin-binding proteins and studies on the expression of fnb genes. *Mol. Microbiol.* **17,** 1143–1152 (1995).
12. Potts, J. R., Bright, J. R., Bolton, D., Pickford, A. R. & Campbell, I. D. Solution structure of the N-terminal F1 module pair from human fibronectin. *Biochemistry* **38,** 8304–8312 (1999).
13. Jaffe, J., Natanson-Yaron, S., Caparon, M. G. & Hanski, E. Protein F2, a novel fibronectin-binding protein from *Streptococcus pyogenes*, possesses two binding domains. *Mol. Microbiol.* **21,** 373–384 (1996).
14. Penkett, C. J. *et al.* Identification of residues involved in the interaction of *Staphylococcus aureus* fibronectin-binding protein with the ^{4}F1^{5}F1 module pair of human fibronectin using heteronuclear NMR spectroscopy. *Biochemistry* **39,** 2887–2893 (2000).
15. Talay, S. R., Valentin-Weigand, P., Jerlstrom, P. G., Timmis, K. N. & Chhatwal, G. S. Fibronectin-binding protein of *Streptococcus pyogenes*—sequence of the binding domain involved in adherence of streptococci to epithelial cells. *Infect. Immun.* **60,** 3837–3844 (1992).
16. Signäs, C. *et al.* Nucleotide sequence of the gene for a fibronectin-binding protein from *Staphylococcus aureus*—use of this peptide sequence in the synthesis of biologically-active peptides. *Proc. Natl Acad. Sci. USA* **86,** 699–703 (1989).
17. Schwarz-Linek, U. *et al.* Binding of a peptide from a *Streptococcus dysgalactiae* MSCRAMM to the N-terminal F1 module pair of human fibronectin involves both modules. *FEBS Lett.* **497,** 137–140 (2001).
18. Huff, S., Matsuka, Y. V., McGavin, M. J. & Ingham, K. C. Interaction of N-terminal fragments of fibronectin with synthetic and recombinant D motifs from its binding protein on *Staphylococcus aureus* studied using fluorescence anisotropy. *J. Biol. Chem.* **269,** 15563–15570 (1994).
19. Massey, R. C. *et al.* Fibronectin-binding protein A of *Staphylococcus aureus* has multiple, substituting, binding regions that mediate adherence to fibronectin and invasion of endothelial cells. *Cell. Microbiol.* **3,** 839–851 (2001).
20. Talay, S. R. *et al.* Co-operative binding of human fibronectin to SfbI protein triggers streptococcal invasion into respiratory epithelial cells. *Cell. Microbiol.* **2,** 521–535 (2000).
21. Derrick, J. P. & Wigley, D. B. Crystal structure of a streptococcal protein-G domain bound to an Fab fragment. *Nature* **359,** 752–754 (1992).
22. Pickford, A., Smith, S., Staunton, D., Boyd, J. & Campbell, I. The hairpin structure of the ^{6}F1^{1}F2^{2}F2 fragment from human fibronectin enhances gelatin binding. *EMBO J.* **20,** 1519–1529 (2001).
23. Cornilescu, G., Delaglio, F. & Bax, A. Protein backbone angle restraints from searching a database for chemical shift and sequence homology. *J. Biomol. NMR* **13,** 289–302 (1999).
24. Brünger, A. T. *X-PLOR (Version 3.1) A System for X-ray Crystallography and NMR* (Yale University, New Haven, Connecticut, 1992).
25. Sass, H. J., Musco, G., Stahl, S. J., Wingfield, P. T. & Grzesiek, S. Solution NMR of proteins within polyacrylamide gels: Diffusional properties and residual alignment by mechanical stress or embedding of oriented purple membranes. *J. Biomol. NMR* **18,** 303–309 (2000).

26. Ottiger, M., Delaglio, F. & Bax, A. Measurement of *J* and dipolar couplings from simplified two-dimensional NMR spectra. *J. Magn. Reson.* **131,** 373–378 (1998).
27. Hashimoto, Y. *et al.* The relative orientation of the fibronectin ^{6}F1^{1}F2 module pair: A N-15 NMR relaxation study. *J. Biomol. NMR* **17,** 203–214 (2000).
28. Tjandra, N., Garrett, D. S., Gronenborn, A. M., Bax, A. & Clore, G. M. Defining long range order in NMR structure determination from the dependence of heteronuclear relaxation times on rotational diffusion anisotropy. *Nature Struct. Biol.* **4,** 443–449 (1997).
29. Wishart, D. S., Sykes, B. D. & Richards, F. M. The chemical-shift index—a fast and simple method for the assignment of protein secondary structure through NMR spectroscopy. *Biochemistry* **31,** 1647–1651 (1992).
30. Talay, S. R., Valentin-Weigand, P., Timmis, K. N. & Chhatwal, G. S. Domain-structure and conserved epitopes of Sfb protein, the fibronectin-binding adhesin of *Streptococcus pyogenes*. *Mol. Microbiol.* **13,** 531–539 (1994).

Acknowledgements We thank R. Aplin for mass spectrometry, M. Pitkeathly for peptide synthesis, and S. Lukomski for the *S. pyogenes* M75 DNA (4673). This research was supported by the Wellcome Trust and the Biotechnology and the Biological Sciences Research Council. J.R.P. acknowledges the British Heart Foundation for financial support.

Competing interests statement The authors declare that they have no competing financial interests.

Correspondence and requests for materials should be addressed to J.R.P. (jennifer.potts@bioch.ox.ac.uk). The atomic coordinates have been deposited in the Protein Data Bank with ID code 1O9a.

Nicotinamide and *PNC1* govern lifespan extension by calorie restriction in *Saccharomyces cerevisiae*

Rozalyn M. Anderson*, Kevin J. Bitterman*, Jason G. Wood*, Oliver Medvedik & David A. Sinclair

Department of Pathology, Harvard Medical School, Boston, Massachusetts 02115, USA
* *These authors contributed equally to this work*

Calorie restriction extends lifespan in a broad range of organisms, from yeasts to mammals. Numerous hypotheses have been proposed to explain this phenomenon, including decreased oxidative damage and altered energy metabolism. In Saccharomyces cerevisiae, lifespan extension by calorie restriction requires the NAD$^+$-dependent histone deacetylase, Sir2 (ref. 1). We have recently shown that Sir2 and its closest human homologue SIRT1, a p53 deacetylase, are strongly inhibited by the vitamin B_3 precursor nicotinamide[2]. Here we show that increased expression of *PNC1* (pyrazinamidase/nicotinamidase 1), which encodes an enzyme that deaminates nicotinamide, is both necessary and sufficient for lifespan extension by calorie restriction and low-intensity stress. We also identify *PNC1* as a longevity gene that is responsive to all stimuli that extend lifespan. We provide evidence that nicotinamide depletion is sufficient to activate Sir2 and that this is the mechanism by which *PNC1* regulates longevity. We conclude that yeast lifespan extension by calorie restriction is the consequence of an active cellular response to a low-intensity stress and speculate that nicotinamide might regulate critical cellular processes in higher organisms.

Lifespan in the budding yeast *S. cerevisiae* is extended by a variety of stimuli such as heat stress, osmotic stress and the restriction of amino acids or glucose[1,3–5]. The latter two regimens are considered to be mimics of calorie restriction in higher organisms. In *S. cerevisiae*, replicative age is defined as the number of divisions that a cell undergoes before dying. The yeast *SIR2* gene, which encodes the founding member of a conserved family of NAD$^+$-dependent deacetylases[6–9], is required for lifespan extension by glucose restriction[1]. Cells with an additional copy of *SIR2* live 30% longer than the wild type, whereas *sir2Δ* strains age prematurely[10] owing to increased recombination at the ribosomal DNA (rDNA) locus[10,11]. The importance of elucidating the yeast *SIR2* pathway is underscored by increasing evidence that Sir2 proteins in higher organisms promote longevity and cell viability[12–15].

Because Sir2 protein levels do not increase in response to calorie restriction[16], lifespan extension must involve an increase in enzymatic activity of Sir2. One hypothesis is that Sir2 is activated by an increased availability of NAD$^+$ (ref. 1). Nicotinamide, a product of the Sir2 reaction[17], is a strong non-competitive inhibitor of Sir2-like enzymes *in vitro*[2,17] and can accelerate yeast ageing by inhibiting Sir2 *in vivo*[2]. Thus an alternative explanation is that Sir2 is regulated by changes in nicotinamide levels.

To explore the latter hypothesis, we focused on *PNC1*, a gene whose product converts nicotinamide to nicotinic acid in the NAD$^+$ salvage pathway (Fig. 1a, b). Most wild-type yeast strains have an average lifespan of 21–23 divisions, with a maximum lifespan of about 40 divisions. A wild-type strain that was calorie restricted (0.5% glucose) or heat stressed (37 °C) exhibited a longer lifespan than an untreated control (2.0% glucose or 30 °C, respectively; Fig. 1c, d). The *sir2Δ* strain had a short lifespan, consistent with previous reports[1,10], and neither calorie restriction (0.5% or 0.1% glucose) nor heat stress extended lifespan in this strain (Fig. 1c, d, and data not shown). The *pnc1Δ* strain did not exhibit a lifespan extension under either of these conditions, demonstrating that *PNC1* is necessary for lifespan extension by calorie restriction and low-intensity stress.

Strikingly, under non-stressing conditions (2% glucose, 30 °C), a strain with additional copies of *PNC1* (*5×PNC1*) lived 70% longer than the wild type and some cells lived for more than 70 divisions, which is the longest reported lifespan extension in this organism (Fig. 1e). Neither calorie restriction nor heat stress further increased the lifespan of the *5×PNC1* strain (not shown). Deletion of *SIR2* in the *5×PNC1* background shortened lifespan to that of the *sir2Δ* mutant (Fig. 1e). Furthermore, the *pnc1Δ sir2Δ* double mutant had a lifespan similar to that of the *sir2Δ* mutant (Fig. 1e) and its lifespan was unaffected by glucose restriction (not shown). These findings indicate that *PNC1* and *SIR2* function in the same pathway and that *PNC1* increases lifespan through *SIR2*. Together, these results show that *PNC1* is necessary for lifespan extension by both calorie restriction and heat stress, and that additional *PNC1* is sufficient to mimic these stimuli.

Given that additional *PNC1* is sufficient to extend lifespan, we examined whether *PNC1* expression is upregulated in response to stimuli that extend lifespan. We found that Pnc1 levels were greatly induced in a dose-dependent manner by glucose restriction (Fig. 2a) and in cells carrying a *cdc25-10* allele, which mimics calorie restriction[1] (Fig. 2b). *MSN2* and *MSN4*, which encode transcription factors that coordinate the response to carbon source starvation and intense stress, were not required for Pnc1 induction (not shown). This is consistent with the previous observation that these two genes are not required for lifespan extension by glucose restriction[1].

Pnc1 levels were elevated under every other condition known to extend yeast lifespan, including amino acid restriction, salt stress and heat stress (Fig. 2c), in agreement with whole-genome mRNA analyses of stressed yeast cells[18]. Pnc1 activity in extracts from treated cells was correlated with Pnc1 concentrations in western blots (Fig. 2d), showing that these cells have increased rates of nicotinamide hydrolysis.

We and others have previously shown that two other enzymes in the NAD$^+$ salvage pathway, Npt1 (nicotinic acid phosphoribosyltransferase) and Nma2 (nicotinic acid mononucleotide adenylyltransferase), are concentrated in the nucleus[16,19]. Surprisingly, a fusion protein of Pnc1 with green fluorescent protein (Pnc1–GFP) was not only localized in the nucleus and the cytoplasm but was also